Heme Regulates Allosteric Activation of the Slo1 BK Channel

Frank T. Horrigan,[1] Stefan H. Heinemann,[2] and Toshinori Hoshi[1]

[1]Department of Physiology, School of Medicine, University of Pennsylvania, Philadelphia, PA 19104
[2]Molecular and Cellular Biophysics, Medical Faculty of the Friedrich Schiller University Jena, D-07747 Jena, Germany

Large conductance calcium-dependent (Slo1 BK) channels are allosterically activated by membrane depolarization and divalent cations, and possess a rich modulatory repertoire. Recently, intracellular heme has been identified as a potent regulator of Slo1 BK channels (Tang, X.D., R. Xu, M.F. Reynolds, M.L. Garcia, S.H. Heinemann, and T. Hoshi. 2003. *Nature.* 425:531–535). Here we investigated the mechanism of the regulatory action of heme on heterologously expressed Slo1 BK channels by separating the influences of voltage and divalent cations. In the absence of divalent cations, heme generally decreased ionic currents by shifting the channel's G–V curve toward more depolarized voltages and by rendering the curve less steep. In contrast, gating currents remained largely unaffected by heme. Simulations suggest that a decrease in the strength of allosteric coupling between the voltage sensor and the activation gate and a concomitant stabilization of the open state account for the essential features of the heme action in the absence of divalent ions. At saturating levels of divalent cations, heme remained similarly effective with its influence on the G–V simulated by weakening the coupling of both Ca^{2+} binding and voltage sensor activation to channel opening. The results thus show that heme dampens the influence of allosteric activators on the activation gate of the Slo1 BK channel. To account for these effects, we consider the possibility that heme binding alters the structure of the RCK gating ring and thereby disrupts both Ca^{2+}- and voltage-dependent gating as well as intrinsic stability of the open state.

The Journal of General Physiology

INTRODUCTION

Heme, composed of an iron center and a surrounding protoporphyrin IX, plays critical roles in protein function. Many proteins, including hemoglobin, cytochromes and soluble guanylate cyclases, contain heme as a functionally indispensable prosthetic group. The presence of heme often confers novel properties to the proteins, such as high sensitivity to biologically important gases, including oxygen, nitric oxide, and carbon monoxide (Rodgers, 1999; Jain and Chan, 2003).

While the majority of cellular heme may be bound to proteins, some "uncommitted" or "free" heme likely exists (Ponka, 1999). Precise estimates of free intracellular heme concentration are not widely available because of technical problems, but an estimate of >1 μM has been reported for reticulocytes (Garrick et al., 1999). In neuronal cells, intracellular heme concentration may dramatically increase following hemorrhagic strokes. These vascular accidents lead to a breakdown of hemoglobin and release of heme in the extracellular medium (Wagner and Dwyer, 2004). Extracellular heme is transported across the cell membrane by a protenacious mechanism, thereby increasing the intracellular concentration (Worthington et al., 2001).

Increasing evidence suggests that intracellular heme acts as a signaling molecule (Padmanaban et al., 1989). For example, heme reversibly binds to selected transcription factors and initiates cellular signal transduction events involving diverse classes of proteins (Zhang and Hach, 1999). Aside from the selected heme-binding transcription factors, how other proteins involved in signal transduction, such as ion channels, are acutely regulated by heme is not well understood. As a first step toward identification of the effectors of intracellular heme, we have recently shown that heme binds to a cytoplasmic domain of a large conductance Ca^{2+}-dependent potassium (Slo1 BK) channels, a key inhibitory component in neuronal and muscle excitability, and drastically reduces the channel activity (Tang et al., 2003). While the detailed mechanism of the heme-mediated inhibition of heterologously expressed Slo1 BK channels is not yet known, the effect is exquisitely potent, with a typical IC_{50} value of <80 nM. This high sensitivity suggests that heme or a heme-like endogenous substance may be a potent modulator of Slo1 BK channels, especially during "heme stress," such as that following hemorrhagic strokes (Wagner and Dwyer, 2004). Such injuries are often followed by cerebral vasospasm, in which an inhibition of the Slo1 BK channel function may play a critical role (Aihara et al., 2004; Williams et al., 2004).

Gating of the Slo1 BK channel is allosterically controlled by voltage and divalent cations (e.g., Cox et al., 1997; Rothberg and Magleby, 2000; summarized in Magleby, 2003; Rothberg, 2004). The activation gate of the Slo1 BK channel may be opened by depolarization alone without Ca^{2+}, or Ca^{2+} alone without depolarization, but under physiological conditions, both Ca^{2+} and

Correspondence to Toshinori Hoshi: hoshi@hoshi.org

depolarization work synergistically to activate the channel (Cui et al., 1997). This multidimensional allosteric characteristic allows Slo1 BK channels to participate in multitudes of physiological phenomena, generally exerting a finely tuned negative influence on cellular excitability (Sah, 1996; Vergara et al., 1998).

The physiological versatility of the Slo1 BK channel based on its multidimensional allosteric property complicates studies of its modulation. A given modulator, such as heme, may alter the channel function by affecting any one of the allosteric interactions, and its overall effect may be excitatory or inhibitory, depending on voltage and the divalent ion concentration. Here we investigated how heme inhibits the Slo1 BK channel by separating the influences of voltage and divalent cations. Measurements and simulations of ionic and gating currents show that heme decreases the allosteric coupling of voltage sensor activation and Ca^{2+} binding to channel opening.

MATERIALS AND METHODS

Channel Expression

For ionic current measurements, human Slo1 (hSlo1) BK channels (U11058) were expressed transiently in HEK-tsA cells using the FuGene method (Roche) as previously described (Avdonin et al., 2003). The cells were used for electrophysiological experiments typically within 18–36 h of transfection. For gating current measurements, mouse Slo1 (mSlo1) (Horrigan and Aldrich, 2002) was heterologously expressed in HEK-tsA cells.

Ionic Current Measurements

Macroscopic and single-channel ionic currents were recorded in the inside-out configuration using an AxoPatch 200B amplifier (Axon Instruments) essentially as previously described (Tang et al., 2001; Avdonin et al., 2003). When filled with the solutions described below, the typical input resistance of electrodes for macroscopic currents was 1.5 MΩ while that for single-channel currents was >3 MΩ. Approximately 1.2 MΩ of the series resistance was electronically compensated in the macroscopic recordings. Typically, macroscopic tail currents started to decay exponentially within 60–70 μs of a voltage step and the initial 100-μs segments were excluded from analysis. Unless otherwise stated, macroscopic capacitative and leak currents were subtracted using a *P*/6 protocol from the leak holding voltage of −50 mV. When necessary, single-channel records without any openings were used to subtract single-channel leak and capacitative components. Both macroscopic and single-channel data were filtered through the built-in filter circuit of the patch-clamp amplifier at 10 kHz and digitized at 100 kHz (ITC16; Instrutech). Data acquisition was controlled by a custom software (PatchMachine) (Tang et al., 2001, 2004; Avdonin et al., 2003) running on Mac OS 10.

Composite single-channel i–V curves were obtained using voltage ramp protocols (Hoshi, 1995). In brief, this involved averaging different segments of data recorded in response to ramp depolarization into different bins. Typically, openings were elicited by voltage ramp stimulation from 0 to 240 mV and then back to 0 mV in 10 ms.

Gating Current Measurements

Gating currents were measured as previously described (Horrigan and Aldrich, 2002). In brief, inside-out patches expressing mSlo1 channels were excised into nominally K^+-free solutions containing isotonic TEA in the extracellular solution to block any residual ionic currents. Voltage commands were filtered at 20 kHz to limit capacitive transients. Currents were filtered at 20 kHz, sampled at 200 kHz, and leak subtracted using a *P*/−4 protocol.

Solutions

For ionic current measurements, the extracellular solution contained (in mM) 140 KCl, 2 $MgCl_2$, 10 HEPES, pH 7.2 with NMDG. The "zero" divalent internal solution contained (in mM) 140 KCl, 11 EGTA, 10 HEPES, pH 7.2 with NMDG. The internal solution with 1 μM [Ca^{2+}] contained (in mM) 140 KCl, 10 HEDTA, 2.4 $CaCl_2$, 10 HEPES, pH 7.2 with NMG. The "saturating" Ca^{2+}/Mg^{2+} solution contained (in mM) 140 KCl, 10 $MgCl_2$, 0.12 $CaCl_2$, 10 HEPES, pH 7.2 with NMG. Free [Ca^{2+}] levels were calculated by Patcher's Power Tools v1.0 (F. Mendez; http://www.mpibpc.gwdg.de/abteilungen/140/software/).

For gating current measurements, the extracellular solution contained (in mM) 130 TEA, 20 HEPES, 2 $MgCl_2$, 6 HCl, pH 7.2 with methanesulfonic acid (MES). The internal solution contained (in mM) 140 NMDG, 5 EGTA, 20 HEPES, 25 HCl, pH 7.2 with MES.

Heme was applied in the form of iron protoporphyrin IX chloride (hemin; Sigma-Aldrich). Heme was dissolved, diluted with the desired internal solution to 10 μM, and stored at −80°C. For each experiment, a fresh tube was thawed immediately before use and diluted to the final concentrations. Electrophysiology experiments with heme were performed with a minimum of illumination. To change the bath heme concentration, the recording chamber (∼150 μl) was washed with 1 ml of a new solution and 4 min was allowed to elapse before measurements. The effects of heme were partially reversible with wash but the recovery time course was variable. The time course observed was generally faster than that reported by Tang et al. (2003). It is not clear what accounts for the difference. To obtain concentration dependence data, each patch was treated with increasing concentrations of heme.

Data Analysis

Data were analyzed using PatchMachine (Tang et al., 2001, 2004; Avdonin et al., 2003) and IgorPro (Wavemetrics) running on Mac OS 10. Tail currents at −40 mV following pulses to different voltages were fit with a single exponential to extrapolate instantaneous current amplitudes. The voltage dependence of the instantaneous current size was then fit with a Boltzmann equation to estimate the maximum macroscopic conductance (G_{max}) values and the normalized G–V curve. Macroscopic kinetics of Slo1 currents was characterized using a single exponential, and the voltage dependence of the time constant was in turn fitted with an exponential function. To measure open probability and dwell times, the openings were idealized using the hidden Markov method as implemented in PatchMachine (Avdonin et al., 2000). First latency distributions were corrected for the number of channels present (Aldrich et al., 1983), and the fractional number of blank sweeps is obtained from the corrected distribution. The free energy contribution of divalent ions to channel activation was determined using the formulation of Cui and Aldrich (2000) as implemented previously (Tang et al., 2004). Gating current data were analyzed as described in Horrigan and Aldrich (2002).

Simulation

Simulated currents were generated and analyzed using PatchMachine and IgorPro as performed with experimental data. The effects of leak and capacitance subtraction, series resistance, and the built-in filter of the amplifier were not considered. The single-channel conductance was set at 250 pS. Simulated single-channel data contained Gaussian noise whose RMS noise level corresponded to that of typical experimental data (1 pA).

The values of the parameters in the HCA model (Horrigan et al., 1999) were estimated in the following manner. The macroscopic tail kinetics and the open probability values estimated from the single-channel data at extreme negative voltages determined the initial values of γ_0 and L_0. The voltage dependence of the deactivation kinetics at negative voltages determined the partial charge associated with $\gamma_{0\text{-}4}$. The macroscopic activation kinetics at extreme voltages estimated the value of δ_4. Then the values of D, δ_2, and δ_3 (see Fig. 1) were adjusted so that the simulated macroscopic G–V, kinetics of the ionic currents, and the single-channel open probability matched the respective average experimental data as judged by eye. The γ_0 value in this study is smaller than that reported previously for mSlo1 (Horrigan et al., 1999), but it is unclear what accounts for the difference. As in Horrigan et al. (1999), the values of γ_0 and γ_1 were assumed to be the same. The values of δ_2 and δ_3 were adjusted to fit the voltage dependence of the kinetics of macroscopic current relaxation with the constraint that the values of δ's are a monotonic function of voltage. The simulation process did not consider the heme-mediated decrease in the maximum macroscopic conductance.

Simulations of G–V curves based on the model of Horrigan and Aldrich (Horrigan and Aldrich, 2002) involving the full allosteric interactions among the channel gate, voltage sensor, and Ca^{2+} binding were performed using IgorPro. The values of the Ca^{2+}-dependent parameters in the model were taken from Horrigan and Aldrich (2002). The G–V curves predicted by the model of Horrigan and Aldrich were not corrected for the data processing procedure.

Statistics

Statistical comparisons were made using *t* test or paired *t* test as appropriate with DataDesk (Data Description). Statistical significance was assumed at $P \leq 0.05$. Where appropriate, data are presented as mean ± SEM.

RESULTS

The seemingly complex gating of the Slo1 channel may be interpreted using the concept that the channel's gate is allosterically controlled by voltage, and cytoplasmic Ca^{2+} and Mg^{2+} (summarized in Magleby, 2003). In the absence of divalent cations, the Slo1 channel functions essentially as a voltage-dependent channel, and the gating properties are well described by the model of Horrigan et al. (1999) (HCA model) (Fig. 1). The HCA model postulates that the weakly voltage-dependent intrinsic opening/closing processes of the channel gate (vertical transitions) are allosterically regulated by the steeply voltage-dependent movement of the voltage sensor (horizontal transitions). In this study, we used the framework of the HCA model to elucidate the mechanism of the heme action on channel function and performed the initial set of experiments in the virtual absence of divalent cations.

Application of heme (100 nM) to the cytoplasmic side of the channel progressively decreased the Slo1 current size at 160 mV to ~36 ± 19% (n = 17) of the control amplitude with a pseudo second-order rate constant of $2.2 \times 10^5 \pm 1.2 \times 10^4\ s^{-1}*M^{-1}$ (n = 17; Fig. 2 A). As reported earlier (Tang et al., 2003), the fractional inhibition of the current and the time course of

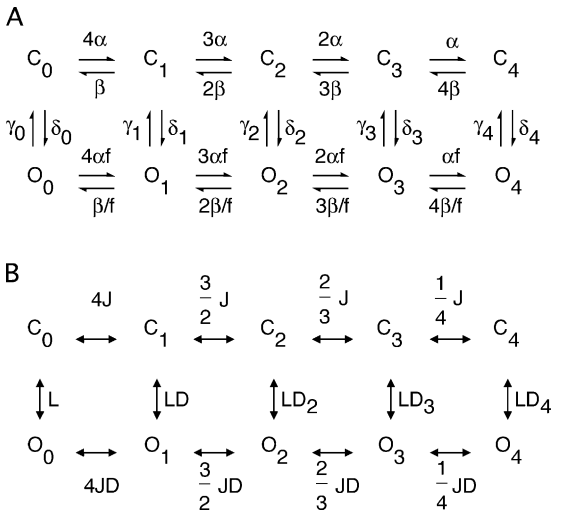

Figure 1. Allosteric gating model of Slo1 in the absence of divalent ions proposed by Horrigan et al. (1999). (A) HCA model with individual rate constants. (B) HCA model using equilibrium constants. The allosteric factor D is defined as $D = f^2$, the weakly voltage-dependent open–closed equilibrium constant is defined as $L_0 = \delta_0/\gamma_0$ at 0 mV, and the strongly voltage-dependent equilibrium constant J is defined as $J = \alpha/\beta$ at 0 mV. For details, see Horrigan et al. (1999). The most likely activation pathway on moderate to large depolarization is C_0-C_1-C_2-C_3-C_4-O_4 and the most likely deactivation pathway on repolarization to a very negative voltage is O_4-O_3-O_2-O_1-O_0-C_0.

the development of the current inhibition were notably variable among the patches examined. When heme was applied without repeated depolarization (Fig. 2 B), the fractional inhibition of the current was unaltered (~21 ± 14%, n = 3, P = 0.17). The effectiveness of heme in the absence of divalent ions suggested that the underlying mechanism likely involved the intrinsic and/or voltage-dependent gating of the Slo1 channel. Furthermore, the inhibitory efficacy of heme did not require depolarization-mediated channel opening.

The reduction of the current size caused by heme was accompanied by a consistent slowing of the deactivation process at −100 mV (Fig. 2 C). The tail currents at −100 mV were well described by a single exponential with a time constant of 0.19 ± 0.08 ms (n = 24) in the control condition (Fig. 2 C), and application of heme increased the time constant value by ~81 ± 13% ($P \leq 0.001$). This slowing of the deactivation kinetics will be described in detail later (see Fig. 8).

Open-channel i–V

Despite the dramatic reduction in the macroscopic current described above, the open-channel i–V properties of Slo1 remained largely unaltered. The composite i–V curves for the main conductance state in the control condition and the experimental condition with heme (100 nM; Fig. 3 A, left and right sweeps 1 and 2) were indistinguishable (Fig. 3 B). However, in the presence

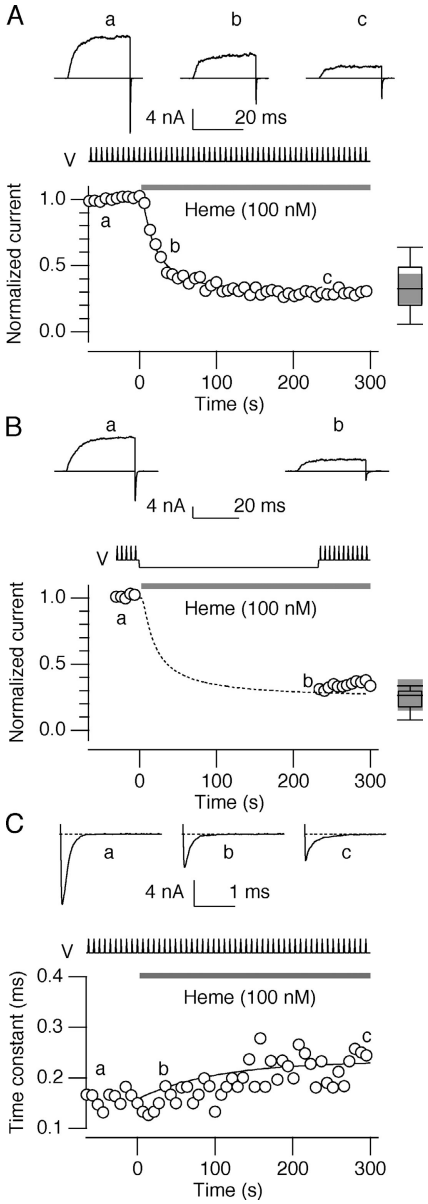

Figure 2. Time course of Slo1 inhibition by heme in the absence of divalent ions. (A) Heme (100 nM) progressively reduced Slo1 currents elicited by pulses from 0 to 160 mV every 6 s. The normalized macroscopic conductance is ~0.5 at this voltage. The scaled peak current amplitude is plotted as a function of time. Representative sweeps obtained at different times (a, b, and c) are also shown. The smooth curve is a single exponential fit to the data with a time constant of 24 s. The boxplot on the right summarizes the fractional inhibition of currents from 17 patches. (B) Inhibitory effect of heme (100 nM) persists without depolarization. The patch was held at −80 mV during the first 4 min after heme application. The dashed curve represents the exponential fit to the data shown in A. (C) Heme (100 nM) slows the tail current time course at −100 mV. The smooth curve is a single exponential curve with a time constant of 10 s. The data were obtained from the same patch as in A. Inset shows representative tail currents obtained at different times (a, b, and c).

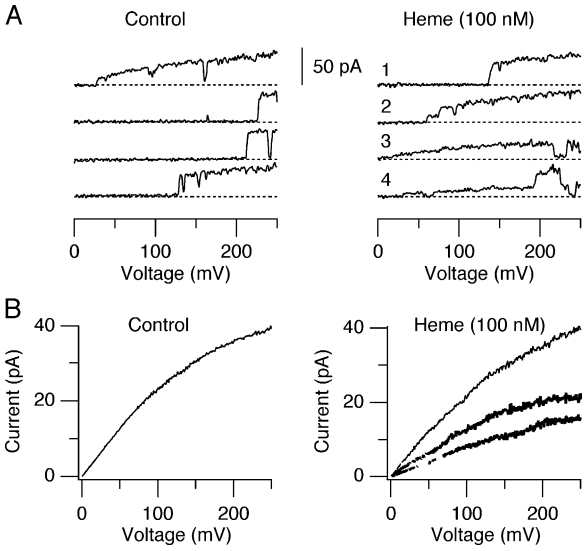

Figure 3. Open-channel i–V is not markedly altered by heme. (A) Channel openings elicited by ramp depolarization from 0 to 240 mV in the control condition (left) and with 100 nM heme (right). The sweeps designated by 1 and 2 show the main conductance level. The sweep designated by 3 shows the 60% substate and that by 4 illustrates the 40% substate. (B) Composite i-V curves obtained by conditional averaging of many openings as shown in A.

of heme, smaller conductance levels, corresponding to ~60 and 40% of the full level (Fig. 3 A, sweeps 3 and 4), were more frequently observed. The increased occurrence of these substates was unequivocal, but the extent of the increase was, however, variable from one patch to the next and difficult to quantify. The rectification properties of these substates were not markedly different from those of the main state. While the occurrence of these substates probably contributed to the macroscopic current inhibition by heme, most of the inhibitory effect of heme was likely mediated by changes in the channel gating as described below.

Slo1 Channels with Heme Open with Depolarization

Heme (100 nM) inhibited Slo1 currents recorded at a variety of voltages (Fig. 4 A), but even in the presence of heme, greater depolarization elicited larger and more rapidly activating currents (Fig. 4, A and B). Comparison of the normalized macroscopic G–V curves inferred from tail current measurements before and after heme application showed that the channels in the presence of heme retained depolarization-activated gating (Fig. 4 C). The normalized G–V curve obtained in the presence of heme was well described by a simple Boltzmann function but it was noticeably shallower and shifted to the right along the voltage axis.

A Single Population of Channels

The kinetics of the tail currents was invariant with the prepulse voltage both without and with heme (Fig. 4

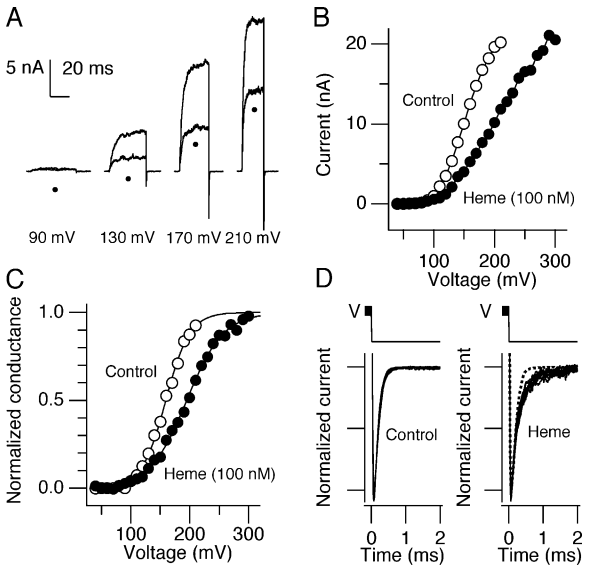

Figure 4. Slo1 channels open with depolarization in the presence of heme. (A) Representative Slo1 currents recorded at different voltages before and after application of heme (100 nM; thick sweeps, denoted with •). (B) Representative peak I–V curves obtained from outward currents. (C) Representative normalized macroscopic G–V curves obtained from tail currents. The smooth lines represent Boltzmann fits to the data. The values of $V_{0.5}$ and Q_{app} for the control group were 160 mV and 1.2 *e* and those for the heme group were 198 mV and 0.77 *e* (see Fig. 6 for more). (D) Scaled tail currents at −180 mV following pulses to 120 to 220 mV in 10 mV increments before (left) and after (right) application of heme (100 nM). In each condition, the currents, 11 sweeps, essentially superimpose and the currents recorded with heme are slower than the control currents. The dotted trace in right shows the tail current time course in the control condition without heme. Data in A, B, and C are from the same patch.

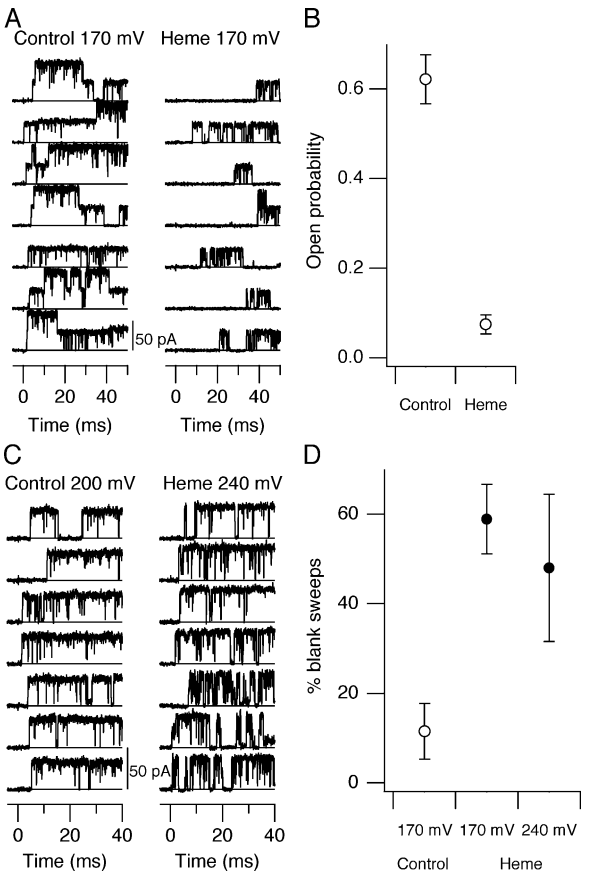

Figure 5. Inhibition of single-channel openings by heme. (A) Representative openings elicited by pulses to 170 mV before and after application of heme (100 nM). Pulses were applied every 2 s. (B) Decrease in the peak open probability at 170 mV by heme (100 nM). All single-channel traces were included in the analysis. (C) Selected openings elicited by pulses to 200 mV in the control condition (left) and those by pulses to 240 mV with heme (100 nM; right). (D) Fractional numbers of blank sweeps observed at 170 mV without heme (left), at 170 mV with heme (100 nM; center), and at 240 mV with heme (100 nM; right). Pulses (≥50 ms at 170 mV and ≥40 ms at 240 mV) were applied every 2 s. The fractional numbers of blank sweeps were calculated from the first latency distributions corrected for the number of channels. A typical distribution contained ≥100 events.

D). For example, in the presence of heme, the time course of the tail current following a prepulse to 120 mV, where the normalized conductance value was ~0.1 was virtually identical to that following 220 mV, where the normalized conductance was ~0.75. Similar results were obtained using different prepulse voltages, tail voltages, and heme concentrations (≥100 nM). The invariance of the tail kinetics from the prepulse voltage suggests that a kinetically single population of channels contributes to the shallower G–V curve observed with heme at ≥100 nM (Swartz and MacKinnon, 1997); the shallower G–V does not result from activation of unmodified channels at the foot of the G–V and heme-bound channels at more positive voltages.

Single-channel Gating

Consistent with the idea that heme alters the gating of Slo1, application of heme (100 nM) drastically decreased the peak open probability (Fig. 5). At 170 mV, heme decreased the peak probability value from 0.62 ± 0.05 to 0.08 ± 0.02 ($P \leq 0.0001$). The decrease in open probability was accompanied by a significant decrease in the mean open duration from 2.3 ± 0.3 to 0.70 ± 0.17 ms ($P = 0.004$).

With large depolarization, the maximum open probability of Slo1 in the control condition saturated at ~0.8–0.9 (200 mV in Fig. 5 C). Qualitatively similar openings were also observed in the presence of heme (100 nM) but greater depolarization (240 mV in Fig. 5 C) was required. The absolute maximum open probability was slightly lower because of the greater occurrence of short flicker closures. Nonetheless, the Slo1 channel in the presence of heme retained the ability to open.

More notably, heme significantly increased the number of blank sweeps (depolarization epochs during which a channel failed to open) (Fig. 5 D). In the con-

trol condition, ~10% of the pulses to 170 mV (≥50 ms in duration) failed to elicit at least one opening. In the presence of heme (100 nM), up to 60% of the pulses to 170 mV produced no opening. Greater depolarization to 240 mV (≥40 ms), where the normalized macroscopic conductance is 0.85–0.9 (Fig. 4 C), did not appreciably decrease the number of blank sweeps (Fig. 5 D). As shown later, these pulse durations (≥40 ms) were at least 10 times greater than the time constant of the macroscopic current activation (see Fig. 8). The presence of these blank sweeps suggested that heme remained functionally associated with the channels even at extreme positive voltages and contributed to the macroscopic current inhibition.

The blank sweeps are likely the result of a very slow gating component and they might be eliminated if the depolarization duration was increased. However, the patch instability associated with repeated extreme depolarization prevented us from testing this idea. In some macroscopic currents, we observed but did not quantify a minor and variable slow component.

Dependence of Macroscopic G–V on Heme Concentration

Heme progressively inhibited the currents recorded at >50 mV in a concentration-dependent manner (Fig. 6 A). Even in the presence of heme, the macroscopic conductance saturated with very large depolarization. This is illustrated in Fig. 6 B where the tail currents recorded at −40 mV following prepulses to different voltages pulses are shown superimposed. Depolarization to >350 mV did not further increase the tail current, indicating that the macroscopic conductance saturated.

As predicted from the single-channel observation that heme increased the number of blank sweeps, heme decreased macroscopic apparent G_{max} estimated from the tail current size (Fig. 6 C). The decrease in G_{max} was notably variable, but a 40–50% decrease was typically observed with heme (≥100 nM) (Fig. 6 C). This reduction is similar to the fractional number of blank sweeps observed in the single-channel data (Fig. 5).

When the G–V curves were normalized to infer the properties of the channels that opened in the presence of heme, we found that the inhibition of the Slo1 current was accompanied by shallower and right-shifted normalized G–Vs (Fig. 6 D). Each normalized G–V curve was characterized by a simple Boltzmann function as a data descriptor function, and the values of the two parameters, $V_{0.5}$ and the apparent charge movement (Q_{app}), are summarized in Fig. 6 (E and F). The rightward shift of G–V became noticeable starting at ~30 nM heme, which produced a 20 mV shift in $V_{0.5}$. The shift saturated with 300 nM heme, producing a $V_{0.5}$ shift of 80 to 100 mV. Concomitantly with the rightward shift in $V_{0.5}$, heme also decreased Q_{app} so that the G–V curves were markedly shallower. The effect of heme in

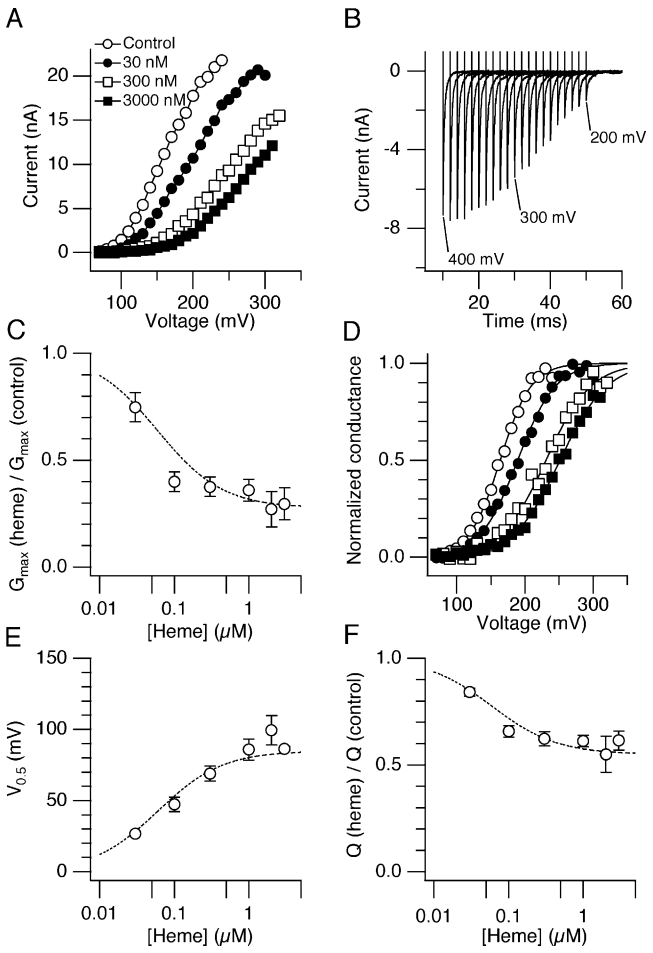

Figure 6. Concentration dependence of the inhibitory effect of heme. (A) Peak I–V curves obtained with different concentrations of heme in a representative patch. (B) Tail currents recorded at −40 mV saturate in size following pulses to 200 to 400 mV in 10 mV increments in the presence of 1 μM heme. The pulse to 200 mV was 50 ms in duration, and the duration decreased by 2 ms for each 10 mV increment so that the rightmost tail current was recorded following depolarization to 200 mV and the leftmost current was recorded following depolarization to 400 mV. (C) Changes in G_{max} caused by different concentrations of heme. To limit prolonged extreme depolarization, the pulse duration decreased by 2 ms for every 10 mV depolarization starting from a 75 ms pulse to 0 mV. (C) Normalized macroscopic G–V curves obtained from the currents shown in A. The symbols are as in A. (D) Changes in $V_{0.5}$ by different concentrations of heme. The mean $V_{0.5}$ value in the control condition was 155 ± 2 mV. (E) Fractional changes in Q_{app} by different concentrations of heme. The mean Q_{app} value in the control condition was 1.2 ± 0.04 *e*. Smooth curves in B, C, and D reflect K_d = 60 nM assuming a single binding site. n = 3–20.

reducing Q_{app} saturated around 100 nM, producing a ~40% decrease from 1.2 ± 0.04 *e* in the control condition to 0.78 ± 0.02 *e* (100 nM; Fig. 6 F). It is noteworthy that the decrease in Q_{app} persisted even with the highest concentration of heme tested, supporting the idea that heme-bound channels are characterized by a shallow G–V.

The concentration dependence of the changes in G_{max}, $V_{0.5}$, and Q_{app} was adequately described with an apparent K_d value of 60 nM, assuming binding of one heme molecule was sufficient to induce the effects (Fig. 6, C, E, and F). However, this assumption is not specifically addressed by the results available.

Gating Currents

The changes in G–V caused by heme (Fig. 6) could be explained in several ways. One possibility is that heme directly interferes with the voltage-sensing charge movements involving S4, which are represented by the horizontal transitions in the HCA model (Fig. 1; Horrigan et al., 1999). If these voltage-dependent steps that normally precede channel opening are impeded by heme, ON gating currents (IgON) may be reduced in size and slower at a given voltage. Representative gating currents elicited by brief 0.5-ms pulses from −80 to 200 mV before and after application of heme (300 nM) are compared in Fig. 7 A. This concentration of heme reduced the peak ionic currents by up to 75% (Fig. 6) but had a much smaller effect on the gating currents. The peak IgON and IgOFF were reduced by <15%, and their kinetics were not appreciably altered by heme.

Heme (300 nM) only slightly altered the voltage dependence of the Slo1 gating charge movement (Q_C–V) (Fig. 7 B). Q_C was measured by fitting the first 60–100 μs of the IgON decay with an exponential function and determining the area under the fit (Horrigan and Aldrich, 1999). Slo1 gating currents are much faster than ionic currents, reflecting that voltage sensors are largely equilibrated before channels open. Therefore Q_C indicates the steady-state properties of voltage sensor activation while channels are closed, the top row of horizontal transitions in the HCA model (Fig. 1), reflecting the voltage sensor charge (z_J) and equilibrium constant (J) associated with these transitions.

In the experiment shown, Boltzmann fits to the Q_C–V curves indicated that the gating charge half-activation voltage ($Q_CV_{0.5}$) shifted to more positive voltages by ~20 mV. On average, $Q_CV_{0.5}$ increased by only +22 ± 3 mV (n = 4), which is markedly less than the 80–100 mV shift in $V_{0.5,}$ (see Fig. 6). The total charge movement approximated by the amplitude of the Q_C–V fit (Q_{Cmax}) also decreased slightly (Fig. 7 B). However, this decrease of 7 ± 2% (n = 4) was small compared with the effect of heme on G_{max} (Fig. 6 C). The Q_C–V curves in the presence and absence of heme were well fit by Boltzmann functions with identical voltage sensor charge (z_J = 0.58 e) (Fig. 7, B and C). The value of z_J was fixed to the mean value determined from many control experiments (Horrigan and Aldrich, 1999) because z_J determined from individual experiments is very sensitive to scatter in the data and, if allowed to vary, would obscure small changes in $Q_CV_{0.5}$ and Q_{Cmax}. It is clear from Fig. 7 (B and C) that any change in z_J, if any, must be small and cannot account for the reduced steepness of the G–V. If the ~40% decrease in Q_{app} resulted from a 40% reduction in voltage sensor charge, then a decrease in the limiting logarithmic slope of Q_C–V, which is directly proportional to z_J, would be clearly evident (Fig. 7 C, dashed trace). Similarly, the failure to observe a large decrease in Q_{Cmax} (Fig. 7 B) is inconsistent with a large decrease in z_J.

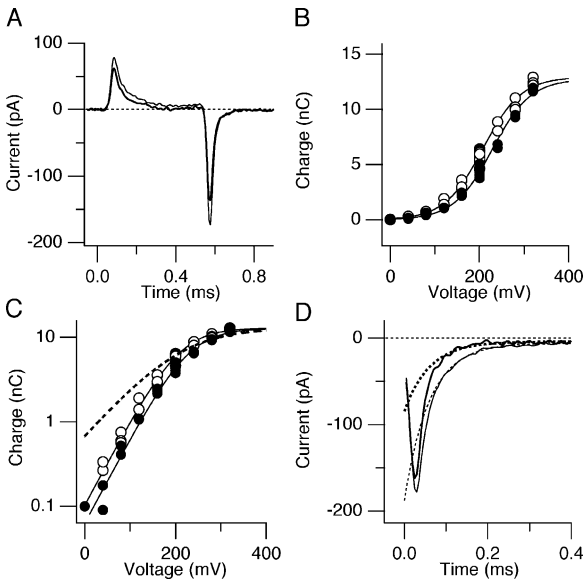

Figure 7. Heme does not markedly alter Slo1 gating currents. (A) Representative gating currents elicited by depolarization from −80 mV to 200 mV before (thin) and after (thick sweep) heme (300 nM). Note that the stimulation duration used is too short to noticeably activate ionic currents. (B) Q_C–V is only slightly affected by heme. Smooth traces are fits to Boltzmann functions with voltage sensor charge z_J = 0.58 e (control, open symbol, $Q_CV_{0.5}$ = 207.5 mV, Q_{Cmax} = 13.4 nC; heme, filled symbol, $Q_CV_{0.5}$ = 228.0 mV, Q_{Cmax} = 12.8 nC). (C) Q_c–V from B is plotted on a semilog scale to show that the limiting slope is not appreciably altered and is inconsistent with a 40% decrease in z_J to 0.35 (dashed trace) analogous to the 40% decrease in G–V slope produced by heme. (D) The slow component of IgOFF (dashed lines) following prolonged depolarization to +200 mV is reduced by heme, consistent with a marked decrease in open probability. Traces represent the average IgOFF following pulses of 5, 10, 15, and 20 ms duration. Individual records were indistinguishable for pulses of 5 ms or longer. A, B, C, and D were all from the same patch.

The effects of heme on Q_c were small and may even be overestimated by our experiments. Small slow decreases in Q_{Cmax} and/or positive shifts in $Q_CV_{0.5}$ were sometimes observed in the absence of heme. Because heme acts slowly and is poorly reversible, we could not rule out that such spontaneous effects contribute to the observed changes in Q_C–V (e.g., Fig. 7 B). However, heme did account for at least some of the Q_C–V changes because they were partially reversed by heme washout (unpublished data).

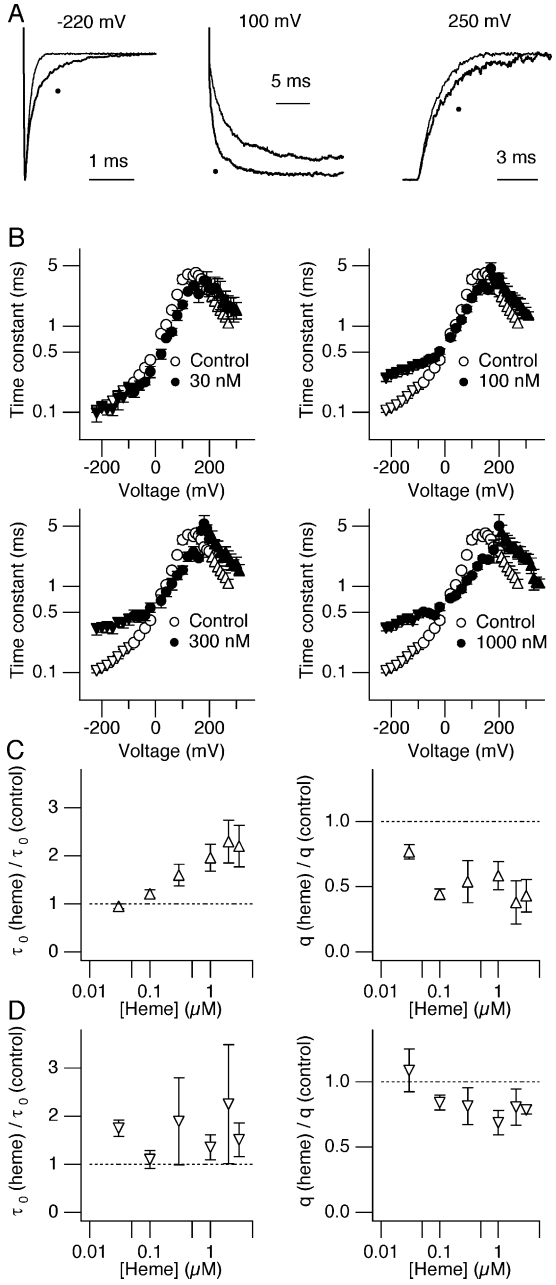

Figure 8. Changes in macroscopic Slo1 kinetics caused by heme. (A) Representative Slo1 currents at −220, 100, and 250 mV before and after heme application. In each set, the current recorded with heme (100 nM) is denoted by • (thick sweep). (B) Voltage dependence of the time constant of current relaxation at different concentrations of heme. Currents were fitted with single exponentials, and the time constant values are plotted as a function of voltage. (C) Concentration dependence of deactivation kinetics at ≤−100 mV. The estimated deactivation time constant values at ≤−100 mV were fitted with an exponential, and the extrapolated values at 0 mV (τ_0) normalized to the control values are plotted as a function of heme concentration (left). The fractional changes in the equivalent charge (q) movement associated with the deactivation process are also shown (right). The mean values of τ_0 and q in the control condition were 0.35 ± 0.017 ms and 0.14 ± 0.01 *e*. (D) Concentration dependence of activation kinetics at ≥210 mV. The estimated activation time constant values at ≥210 mV were fitted with an exponential and the extrapolated values at 0 mV (τ_0) normalized to the respective control values are plotted as a function of the heme concentration (left). The fractional changes in the equivalent charge movement associated with the activation process are also shown (right). The mean values of τ_0 and q in the control condition were 19.0 ± 3.8 ms and 0.24 ± 0.01 *e*. n = 3–21.

Heme had little effect on gating currents evoked by brief voltage pulses (Fig. 7 A) but it had noticeable effects on IgOFF following prolonged (5–20 ms) depolarization (Fig. 7 D), consistent with the ability of heme to inhibit channel opening. IgOFF was slowed following pulses that open Slo1 channels, reflecting transitions among the bottom row of horizontal transitions in the HCA model (Fig. 1). Consequently, IgOFF decays exponentially following a brief pulse, but an additional slow component, whose amplitude reflects the fraction of open channels, appears following prolonged depolarization (Horrigan and Aldrich, 1999). The slow component of IgOFF (Fig. 7 D, dashed lines) was reduced by >50% by heme (300 nM), indicating a marked decrease in open probability. Thus, the small effects of heme on Q_C do not represent a failure of heme to effectively inhibit channel gating under the conditions used to study gating currents. These results taken together suggest that heme did not markedly impede the voltage sensor function when channels are closed.

Heme Slows Macroscopic Activation and Deactivation

Heme altered the kinetics of Slo1 ionic currents in a voltage-dependent manner (Fig. 8 A). The current relaxation time courses were slower after heme application at extreme negative and positive voltages, but at intermediate voltages they were faster (Fig. 8 A).

The time course of Slo1 current relaxation at each voltage was adequately described by a single exponential and the voltage dependence of the current relaxation time constant (τ–V) is illustrated in Fig. 8 B. Consistent with the previous finding of Horrigan et al. (1999), τ–V in the control group had three exponential components. Each component was characterized by the equation $\tau(V) = \tau_0 * e^{(qF/RT)}$ where τ_0 represents the time constant value at 0 mV and q represents the partial charge movement. The component at extreme negative voltages likely reflects the preferred closing transition O_0 to C_0 and that at extreme positive voltages in part reflects the preferred opening transition C_4 to O_4 in the HCA model (Fig. 1 B). The three exponential components were also clearly observed in the presence of heme (Fig. 8 B). Heme markedly slowed the deactivation process at extreme negative voltages by increasing τ_0 and decreasing q (Fig. 8 C), suggesting that heme slows the O_0 to C_0 transition. Much smaller changes were observed with the activation process at extreme positive voltages (Fig. 8 D).

Heme Increases the Open Probability at Negative Voltages

Heme reduced the steepness of the Slo1 G–V curve (see Fig. 6). If the reduced steepness is maintained at more negative voltages, the G–V curves in the control and experimental conditions may cross over so that the channel open probability may be in fact greater after heme treatment at the negative voltages. A similar prediction about the enhanced open probability with heme can be made from the observation that heme slowed the deactivation kinetics at very negative voltages (Fig. 8). Representative openings recorded before and after application of heme (100 nM) at −50, −100, and −150 mV, where the voltage sensor–mediated activation of the channel should be negligible, are shown in Fig. 9. In contrast with the results obtained at more positive voltages, heme strikingly increased the open probability, typically by ~10–20-fold without a significant change in the voltage dependence (Fig. 9 B). The increase in the open probability was associated with a significant increase in the mean open duration by ~50% ($P < 0.01$; Fig. 9 C) at each voltage. The mean open durations observed at these voltages were smaller than the time constants of the macroscopic tail currents (Fig. 8).

Simulations with the HCA Model

The gating properties of Slo1 in the absence of divalent cations are well simulated by the HCA model (Horrigan et al., 1999). To account for the heme action on Slo1 using the HCA model, we considered the following three lines of observations critical. First, heme decreases the steepness of the G–V but does not markedly affect IgON or Q_c–V. Second, heme increases the open probability at very negative voltages. Third, heme slows the kinetics of activation at extreme positive voltages and deactivation at extreme negative voltages. We did not consider the decreased G_{max} (Fig. 6 C) caused by blank sweeps (Fig. 5) or the small shift in Q_c–$V_{0.5}$ (Fig. 7) in our analysis.

A shallower and right-shifted G–V could be simulated in multiple ways using the HCA model. Changes in the steeply voltage-dependent rate constants α and β (the equilibrium constant J) in the HCA model could induce changes in G–V similar to those experimentally observed. However, because the kinetic and steady-state properties of gating currents were not greatly affected by heme (Fig. 7), we deemed that the changes in α and β were unlikely to underlie the heme effect. Changes in the equilibrium constant between the closed state C_0 and the open state O_0, L_0 in the HCA formulation, could also alter the steepness of G–V. A decrease in L_0 caused by greater γ_0 and/or smaller δ_0 shifts the G–V position and decreases the steepness as found with heme. However, this G–V modification also decreased the open probability at negative voltages, exactly the opposite of what was observed. A decrease in the allosteric factor D in the HCA model decreases the G–V steepness, but this change does not appreciably increase open probability at negative voltages as experimentally observed. Thus, alterations in D or L_0 alone fail to account for the experimental findings.

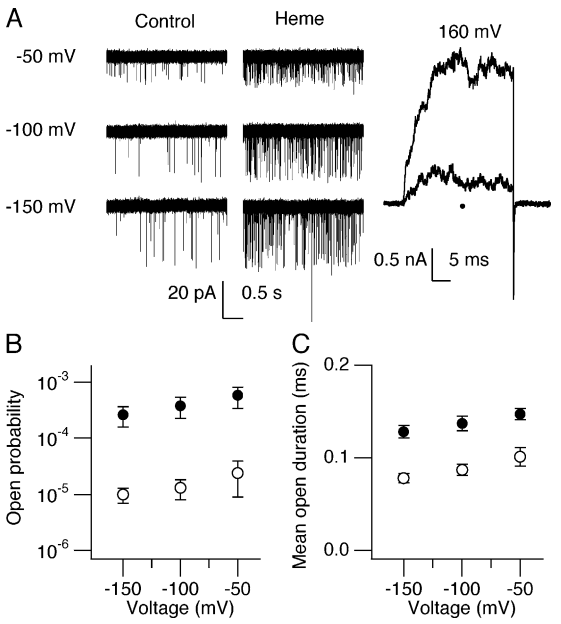

Figure 9. Heme increases the open probability at negative voltages. (A) Representative channel openings at −50, −100, and −150 mV in the control condition and after application of heme (100 nM). Downward deflections represent opening transitions. Heme decreased the current from the same patch at 160 mV (right). The current after heme application is indicated by • (thick sweep). This patch contained ~150 channels assuming the open probability value of 0.5 at 160 mV and the unitary amplitude of 31 pA (see Fig. 3). (B) Voltage dependence of open probability. Open circles, control; filled circles, after heme (100 nM). Typically 60 s data were analyzed. n = 4–6 at each voltage. (C) Voltage dependence of mean open duration. The symbols are as in B. n = 4–6.

However, a decrease in D and a concomitant increase in L_0 together do explain the three key observations listed above. A 73% decrease in D leads to a 45% decrease in Q_{app} and shifts the G–V to more positive voltages (Fig. 10). A 10-fold increase in L_0 accounts for the enhanced open probability, the slower deactivation kinetics, and the longer mean open time at negative voltages (Fig. 10). In addition, the partial charge movement associated with $\gamma_{0\text{-}4}$ is reduced by 50% to account for the reduced voltage dependence of the deactivation time course at very negative voltages. The essential features of the heme action were well simulated using the HCA model by these changes in the following parameters: the allosteric factor D becomes smaller and the equilibrium constant L_0 becomes greater (Fig. 10).

To assess how well other values of D and L_0 simulate the results obtained with heme, the values of D and L_0

A

	Control	Heme	fold change
Allosteric factor D	11.6	3.1	0.27
Closed-open equilibrium constant $L_0 = \delta_0 / \gamma_0$	5×10^{-5}	5×10^{-4}	10
δ_0	0.14 s^{-1}	0.85 s^{-1}	6.1
δ_1	1.62 s^{-1}	2.6 s^{-1}	1.6
δ_2	9.4 s^{-1}	4.1 s^{-1}	0.4
δ_3	55 s^{-1}	7.8 s^{-1}	0.14
δ_4	75 s^{-1}	22 s^{-1}	0.3
Partical charge movement for γ_{0-4}	-0.14 *e*	-0.07 *e*	0.5

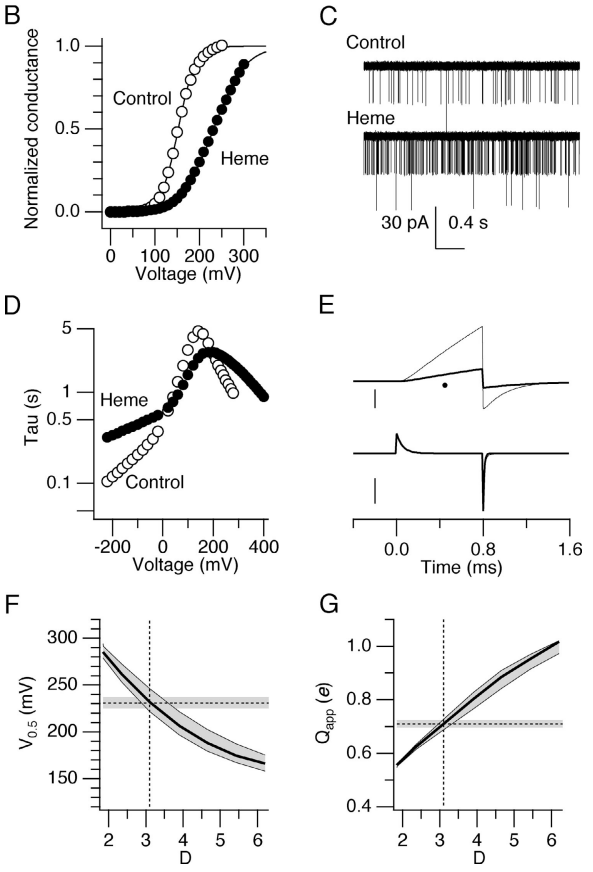

Figure 10. Simulation of the heme action in the absence of divalent ions using the HCA model. (A) The model parameters changed by heme application. The parameter values were adjusted to simulate the average results without heme and with heme (300 nM). As suggested by the results of the gating current measurements, the following parameters were kept constant: $\alpha = 1500\ s^{-1}$, $\beta = 35370\ s^{-1}$, $z_\alpha = 0.275\ e$, and $z_\beta = -0.275\ e$. (B) G–V curves simulated by the model with the parameters shown in A. The values of $V_{0.5}$ and Q_{app} for the simulated control and heme groups were 154 mV/1.3 *e* and 231 mV/0.71 *e*. (C) Simulated single-channel currents at −100 mV. The open probability values for the simulated control and heme groups were 1.6×10^{-5} and 1.5×10^{-4}, and the mean dwell times were 0.24 and 0.45 ms, respectively. (D) Voltage dependence of the simulated macroscopic current relaxation. In A, B, and C, the currents were simulated assuming 250 channels. (E) Simulated ionic and gating currents elicited by depolarization to 200 mV from −100 mV. The top sweep shows ionic currents and the bottom sweep shows gating currents before and after (thick sweeps, denoted by •) heme application. Simulated assuming 20,000 channels. The scale bars represent 700 nA for the ionic currents and 100 pA for the gating currents. (F) Estimated $V_{0.5}$ values as a function of D. The ionic currents were simulated and analyzed using different values of D and L_0. The remaining parameter values are as in A. The thick curve describes how $V_{0.5}$ changes with D using $L_0 = 5 \times 10^{-4}$. The top thin curve describes $V_{0.5}$ changes with $L_0 = 7 \times 10^{-4}$ and the bottom thin curve describes those with $L_0 = 3 \times 10^{-4}$. The area between the two thin curves is shaded gray. The dotted lines indicate the values of D and $V_{0.5}$ as presented in A. The gray horizontal rectangle area represents the standard error associated with the experimentally estimated value of $V_{0.5}$ with 300 nM heme. (G) Estimated Q_{app} values as a function of D. The thick curve describes how Q_{app} changes with D using $L_0 = 5 \times 10^{-4}$. The top thin curve describes Q_{app} changes with $L_0 = 7 \times 10^{-4}$, and the bottom thin curve describes those with $L_0 = 3 \times 10^{-4}$. The dotted lines indicate the values of D and Q_{app} as presented in A. The gray horizontal rectangle area represents the standard error associated with the experimentally estimated value of Q_{app} with 300 nM heme.

are changed and their impacts on $V_{0.5}$ and Q_{app} were evaluated (Fig. 10, F and G). The value of D was varied from 2 to 6 while that of L_0 was varied by ±40%. This range of L_0 corresponds to the fractional standard error associated with the mean estimate of the open probability at −150 mV (Fig. 9), which is the primary determinant of L_0 (Horrigan et al., 1999). Comparison of the range of $V_{0.5}$ simulated in this manner with the experimentally estimated value of $V_{0.5}$ shows that values of D between 2.6 and 3.6 are readily consistent with the experimental results (Fig. 10 F). Similar comparison using Q_{app} also confirms that D is likely to take on a value between 2.7 and 3.4 (Fig. 10 G).

Heme Is Also Effective at Saturating Levels of Ca^{2+} and Mg^{2+}

The virtual absence of Ca^{2+} and Mg^{2+} allowed us to study the effect of heme on the voltage-dependent activation pathway of the Slo1 BK channel in relative isolation. Alternatively, the voltage-dependent gating can be functionally isolated and studied at saturating levels of Ca^{2+} and Mg^{2+}. In the presence of 120 μM [Ca^{2+}] and 10 mM [Mg^{2+}], which are expected to saturate the high- and low-affinity binding sites for divalent ions (Cox et al., 1997; Zhang et al., 2001; Zeng et al., 2005), heme effectively inhibited the currents (Fig. 11 A). As observed in the absence of divalent ions, the tail currents observed with heme saturated following large depolarization (Fig. 11 B). Heme (300 nM) noticeably altered the G–V curve (Fig. 11 C); the $V_{0.5}$ value shifted by 129 ± 9 mV and the Q_{app} value decreased by 40 ± 5.6% to 0.64 *e*. The normalized conductance values at 0 mV (Fig. 11 D) indicated that the channels in the presence of heme (300 nM) were less sensitive to high concentrations of divalent cations; increasing [Ca^{2+}] and [Mg^{2+}] to 120 μM and 10 mM, respectively, produced a much smaller increase in the macroscopic conductance

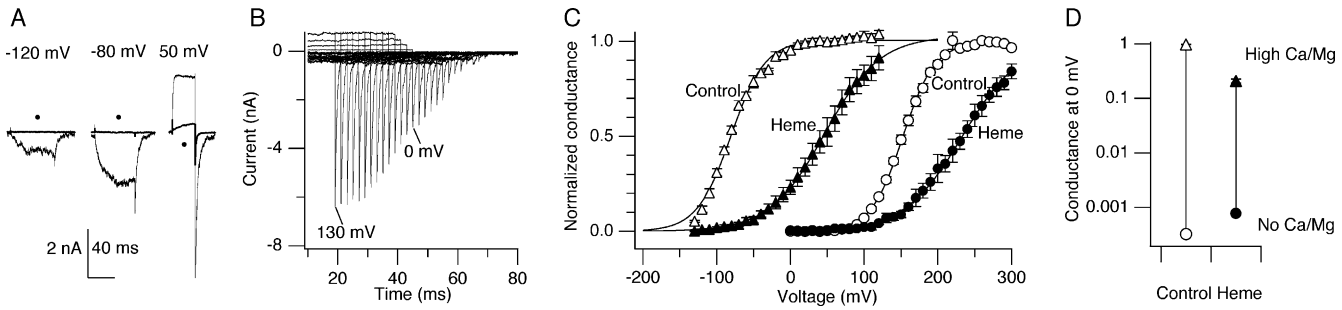

Figure 11. Heme inhibits Slo1 currents in the presence of saturating levels of Ca^{2+} (120 μM) and Mg^{2+} (10 mM). (A) Representative currents at three different voltages before and after heme (100 nM) application with high Ca^{2+}/Mg^{2+}. In each set, the current recorded with heme (300 nM) is denoted by • (thick sweep). No leak or capacitative current subtraction. (B) Tail currents recorded at −160 mV saturate in size following pulses to −150 to 130 mV in 10 mV increments in the presence of 300 nM heme. The pulse to −150 mV was 75 ms in duration, and the duration decreased by 2 ms for each 10 mV increment. (C) Average G–V curves before (open symbols) and after (filled symbols) heme application (300 nM) with high Ca^{2+}/Mg^{2+} (triangles) and with no Ca^{2+}/Mg^{2+} (circles). Tail currents measured at −145 mV were used to estimate G–V with high Ca^{2+}/Mg^{2+}. The estimated values of $V_{0.5}$ and Q_{app} in the control and heme groups with high Ca^{2+}/Mg^{2+} were 80 ± 1.8 mV/1.1 ± 0.08 *e* and 49 ± 9.1 mV/0.64 ± 0.02 *e*, respectively. Without Ca^{2+}/Mg^{2+}, the parameter values were 160 ± 4.3 mV/1.2 ± 0.06 *e* and 229 ± 6.0 mV/0.72 ± 0.01 *e*, respectively. (D) Changes in normalized conductance caused by saturating levels of Ca^{2+} and Mg^{2+}. Average normalized conductance values at 0 mV estimated with no Ca^{2+} and Mg^{2+} and with high $[Ca^{2+}]$ and $[Mg^{2+}]$ before and after heme application (300 nM) are compared. Error bars are smaller than the symbols. $n = 5$ to 8.

when heme was present. Similar inhibitory effects of heme were observed at an intermediate concentration (1 μM) of Ca^{2+} (unpublished data).

With certain assumptions, comparison of the G–V curves recorded in 0 $[Ca^{2+}]$/0 $[Mg^{2+}]$ and 120 μM $[Ca^{2+}]$/10 mM $[Mg^{2+}]$ allows an estimation of the free energy contribution of the divalent ions to the channel activation (Cui and Aldrich, 2000). Such comparison indicates that the presence of heme (300 nM) significantly altered the free energy contribution of the saturating levels of Ca^{2+} and Mg^{2+} ($\Delta G_{Ca/Mg}$) to the channel opening ($P \leq 0.0001$); the mean $\Delta G_{Ca/Mg}$ value decreased by ∼14 ± 1.0 kJ/mol or 51 ± 2.5%, confirming that the Slo1 channel was less sensitive to divalent ions when heme is bound.

Simulations of G-V Curves at High Concentrations of Divalent Cations

The HCA model can be extended to account for the channel behavior in the presence of Ca^{2+} (HA model) (Horrigan and Aldrich, 2002). To simulate the effect of heme on the Slo1 G–V curve at the saturating levels of Ca^{2+} and Mg^{2+} (Fig. 11), the values of the HCA parameters obtained in the absence of divalent ions were applied to the HA model. Because Mg^{2+} was not included in the HA model and for the sake of simplicity, the effect of Mg^{2+} was not considered here. The remaining Ca^{2+}-dependent parameters in the HA model, the Ca^{2+} binding affinity, the allosteric coupling strength between the channel gate and Ca^{2+} binding (C), and the allosteric coupling strength between the voltage sensor and Ca^{2+} binding (E), were initially assumed to be the same in the control and heme conditions, and the values were taken from Horrigan and Aldrich (2002). With this assumption, the HA model predicts that heme increases the channel open probability at $[Ca^{2+}]_i$ = 120 μM (Fig. 12 A), exactly the opposite of what was experimentally observed (Fig. 11). The discrepancy between the experimental and simulation results suggests that heme may alter other aspects of channel gating in addition to D and L_0. Consistent with this possibility, we found that simple decreases in the allosteric coupling strength between the channel gate and Ca^{2+} binding C and that between the voltage sensor and Ca^{2+} binding E by the same fraction as used for D (73%) described the effect of heme on the Slo1 G–V curve at high $[Ca^{2+}]$, at least qualitatively (Fig. 12 B). The simulated steady-state G–V curve in the presence of heme is shifted markedly toward more positive voltages with low as well as high $[Ca^{2+}]$ (Fig. 12), and this is consistent with the experimental results (Fig. 11). It should be noted that the G–V shift in high $[Ca^{2+}]$ is strongly influenced by the allosteric factor C but less so by E. Therefore, it is necessary that C be reduced to reproduce the results in Fig. 11. It is possible that E is changed to a lesser extent or even unchanged. However, the experiments necessary to measure E are outside the scope of this study. Similarly, we did not determine whether heme altered the apparent affinity of Ca^{2+} binding. Such effects, if they occur, are unlikely to account for the reduced response of heme-bound channels to high concentrations of divalent cations in Fig. 11 because the $[Ca^{2+}]$ used (120 μM) was in excess of the normal saturating concentration and channels are still sensitive to low (1 μM) Ca^{2+} in the presence of heme (not depicted). Thus the effects of heme on the Slo1 channel in the absence of divalent ions is consistent with an increase in the closed–open equilibrium

constant L_0 and a decrease in the allosteric coupling factor between the channel gate and the voltage sensor D, and the effects at saturating levels of divalent ions require additional decreases in the Ca^{2+}-dependent allosteric coupling factors C and possibly E.

DISCUSSION

Heme is now emerging as an important intracellular signaling molecule; genomic effects of heme have been reported in several systems and nongenomic effects of heme are beginning to be elucidated. One such example is the acute modulatory effect of heme on the Slo1 BK channel (Tang et al., 2003). Heme reduces ionic currents at depolarized voltages through Slo1 channels in two ways. First, heme decreases G_{max} so that effectively 40–50% less channels open. Second, the channels that open in the presence of heme do so with different characteristics. The G–V curve of the Slo1 channel in the presence of heme is drastically shifted to more positive voltages and less steep. In contrast, Slo1 gating currents remain largely unaffected. At saturating concentrations of divalent cations, the potent efficacy of heme persists.

Interpretations Using the HCA and HA Models

While the overall effect of heme is largely inhibitory at the voltages where the open probability is appreciable, heme exerts an excitatory effect at more negative voltages; the channel open probability is greater when heme is present. Understanding the complex modulatory effects of heme may be facilitated by using well-developed allosteric models of Slo1 channel gating that describe the channel's response to voltage and divalent cations. Simulations of the ionic currents obtained in the absence of divalent ions using the HCA model (Horrigan et al., 1999) suggest that heme markedly decreases the strength of allosteric coupling between the channel gate and the voltage sensor (D) and shifts the equilibrium between the closed and open states in the absence of voltage sensor–mediated activation (L_0) to the open state. The changes in these parameters in conjunction with a decrease in the partial charge movement associated with $\gamma_{0\text{-}4}$ reproduce the salient characteristics of the properties of the Slo1 channels that open in the presence of heme.

The proposed mechanism of heme action based on the HCA model does not consider the decrease in G_{max} (Fig. 6) caused by the blank sweeps in the single-channel data (Fig. 5). Even at very positive voltages with pulses much greater in duration than the macroscopic activation time constant, these blank sweeps are readily observed. They are likely caused by a very slow gating component operating independently of the voltage sensor movement because the total charge movement is only marginally decreased by heme (Fig. 7). The exact nature of this slow gating process and how it relates to the transitions described in the HCA model is not clear. What is certain is that these transitions are not created de novo by heme but their occurrence is drastically increased by heme because a small number of apparent blank sweeps are indeed observed without heme. The channels that do open in the presence of heme kinetically function as a single population, and the contributions from the blanks sweeps and the decrease in G_{max} to our modeling and simulation were likely negligible.

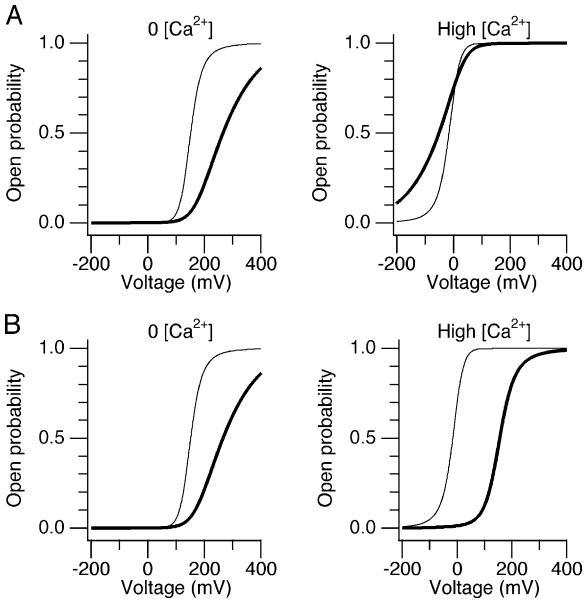

Figure 12. G–V curves simulated by the HA model. (A) Simulated G–V curves at 0 μM (left) and 100 μM Ca^{2+} (right) before (thin curves) and after (thick curves) heme application assuming that heme decreases D by 73% and increases L_0 by a 10-fold as described in Fig. 10. (B) Simulated G–V curves assuming that heme decreases C, D, and E by 73% and increases L_0 by 10-fold.

The modulatory effects of heme on the Slo1 channel persist at saturating levels of Ca^{2+} and Mg^{2+}. Ca^{2+}-dependent gating of the Slo1 channel is successfully described by the HA model (Horrigan and Aldrich, 2002), which builds on the HCA model and incorporates Ca^{2+} as another allosteric dimension. The HA model includes allosteric interactions among the channel gate, voltage sensor, and Ca^{2+}-binding site, and the coupling strengths are described by the parameters C, D, and E. The changes in L_0 and D described for the low-Ca^{2+} condition when incorporated into the HA model do not adequately reproduce the results with high concentrations of divalent cations, suggesting that heme may modulate other functional characteristics of the channel. We find that an across-the-board reduction in C, D, and E by ~70% at least qualitatively reproduces the heme effects at high concentrations of diva-

lent cations. The experiments necessary to rigorously estimate C and E are out of the scope of this study, but the possibility that heme may act as a common regulator of allosteric coupling in Slo1 gating suggests that heme may exert its action where the influences of the voltage sensor and divalent cation binding sites converge.

Molecular Mechanism of Heme Action

The biophysical interpretations of heme action on the Slo1 channel using the HCA and HA models may be given a molecular and structural connotation using the high-resolution structure of the prokaryotic MthK channel (Jiang et al., 2002) and the mechanical spring model of Slo1 gating (Niu et al., 2004). The Ca^{2+}-activated open structure of MthK suggests that the cytoplasmic RCK1 and RCK2 domains in each of the four Slo1 subunits in a channel complex dimerize and that the four RCK dimers in turn form a gating ring structure (Jiang et al., 2002). The expansion and constriction of the gating ring, caused by changes in the relative positions of the four RCK dimers, are envisioned to contribute to channel opening and closing by exerting force on the activation gate through the S6-RCK1 linker (Jiang et al., 2002). The idea that the S6-RCK1 linker exerts mechanical tension on the gate is supported by the observation that open probability, whether Ca^{2+} is absent or present, is drastically influenced by changes in the linker length (Niu et al., 2004). Based on this observation, Niu et al. proposed a mechanical spring model of Slo1 BK channel activation whereby each subunit component of the channel activation gate, likely the cytoplasmic end of S6, is coupled to the cytoplasmic gating ring and also to S4 via two separate spring-like connectors (Armstrong, 2003; Niu et al., 2004). The two separate linkages are required to account for the energetic additivity of voltage and Ca^{2+} in channel activation (Cui and Aldrich, 2000). The highly stylized diagrams in Fig. 13 A capture the essence of the mechanical spring model of Niu et al. (2004) in the absence of Ca^{2+} while incorporating an additional interaction between the voltage sensor and the gating ring composed of the RCK1/RCK2 domains. The presence of voltage sensor/gating ring interaction is consistent with the findings that mutations in S4 and the S4–S5 linker disrupt Mg^{2+}-dependent activation of the channel (Hu et al., 2003) involving the cytoplasmic RCK1 domain (Shi and Cui, 2001; Zhang et al., 2001) and that Mg^{2+} acts to enhance coupling between voltage sensor activation and channel opening (Horrigan, 2005). This model will be used to explain how heme binding to the cytosolic gating ring could influence voltage-dependent gating, and it draws on the idea that a portion of the coupling between voltage sensor and gate may be mediated by interaction between the voltage sensor and gating ring (Hu et al., 2003; Horrigan, 2005).

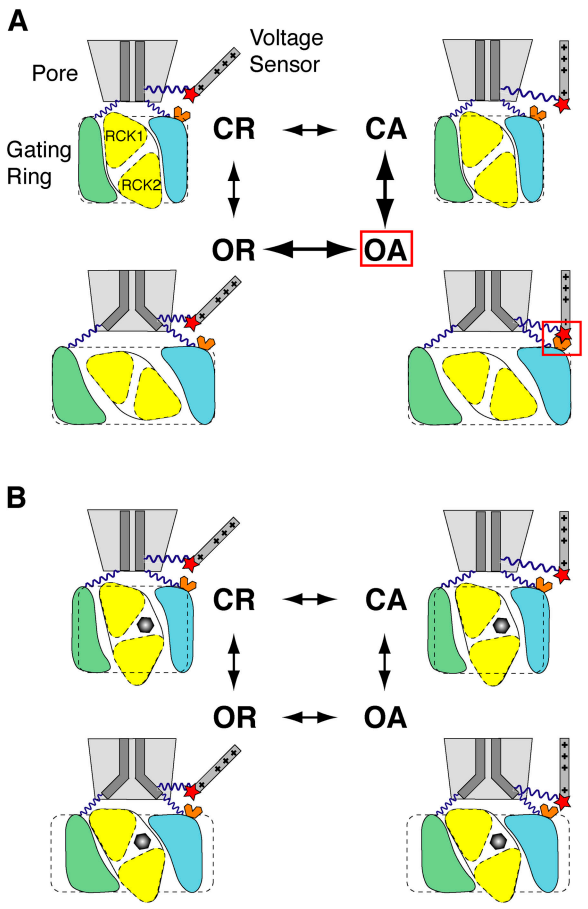

Figure 13. Model of heme action in the absence of Ca^{2+}. Slo1 BK channels in various states of activation are represented by illustrations containing a pore domain whose S6 gate segments are connected by springs to both a charged S4 voltage sensor and a cytoplasmic gating ring. The pore undergoes a closed (C) to open (O) conformational change (vertical transitions) while the voltage sensor undergoes a resting (R) to activated (A) conformational change (horizontal transitions). Only portions of the channel's four subunits are shown, including a single voltage sensor. The states shown (CR, CA, OR, OA) correspond to a single cycle in the HCA model (Fig. 1). Channel opening is associated with expansion of the gating ring, composed of four RCK1/RCK2 dimers. (A) In the absence of heme, the gating ring structure and expansion with channel opening, involving rotation of RCK1/RCK2 dimers, is based on the model of Jiang et al. (2002) for MthK. The expanded gating ring and activated voltage sensor are shown to interact, thereby stabilizing the OA state. (B) Heme binding to the RCK1-RCK2 linker perturbs the RCK1/RCK2 dimer, altering gating ring diameter as compared with the control (dashed boxes) and inhibiting coupling between voltage sensor activation and channel opening by preventing the state-dependent interaction of voltage sensor and gating ring.

In the absence of heme (Fig. 13 A), the pore and gating ring are shown in a closed/constricted (C) or an open/expanded (O) conformation while the charged S4 voltage sensor is depicted in a resting (R) or an acti-

vated (A) state. The voltage sensor interacts with both the activation gate and the gating ring. But the latter interaction is state dependent and occurs only when the gate is open and the voltage sensor is activated (OA state). This state-dependent interaction causes voltage sensor activation to stabilize the open state, functionally equivalent to the interaction represented by the allosteric factor D in the HCA model. Although not depicted, Ca^{2+}, as in the HA model, is assumed to bind with higher affinity to the open/expanded state than to the closed/constricted state, thereby favoring channel activation.

To account for the action of heme, we present the following speculative model that postulates that heme perturbs only the gating ring. We depict heme as binding to the segment between RCK1 and RCK2, altering the structures of the RCK1/RCK2 dimer and of the gating ring (Fig. 13 B). This positioning of heme is consistent with the suggestion by Tang et al. (2003) that heme binding depends on H616 in the RCK1–RCK2 linker segment. We suggest that heme binding makes the constricted conformation of the gating ring less constricted/more expanded, increasing tension on the closed gate to increase L_0. The expanded state of the gating ring may become less expanded, accounting for a decrease in the response to Ca^{2+} (smaller C in the HA model) while also preventing the normal interaction between gating ring and voltage sensor (smaller D in the HA model). By acting on the gating ring, heme may thus act as a common regulator of allosteric coupling.

While speculative, the model in Fig. 13 accounts for the experimental findings presented in this study and is consistent with previous results about Slo1 gating. For example, one key observation is that heme has little impact on gating charge movement when the channels are closed (Fig. 7). This is implemented in the model by postulating that the interaction between voltage sensor and gating ring does not occur in the closed state. The model suggests that heme alters the gating ring structure by perturbing the RCK1/RCK2 dimer interface. This need not be the case but is consistent with the observation of Zhang and Horrigan (2005) that modification of C430 near the dimer interface in the RCK1 domain also alters allosteric coupling for both voltage- and Ca^{2+}-dependent activation.

Some details of the interaction between voltage sensor and gating ring in the model depicted in Fig. 13 are not well constrained by the experimental results. For instance, voltage sensor and gating ring may interact in all states so long as heme impacts these interactions in a state-dependent manner. In addition, a decrease in the allosteric factor D together with an increase in open probability at negative voltages (increasing L_0) could be produced by strengthening interaction between gating ring and voltage sensor in the OR state rather than weakening interaction in the OA state.

The model proposed in Fig. 13 accounts for heme's action as a common regulator of allosteric coupling by postulating that binding of heme to the RCK1/RCK2 linker segment alters the conformational change of the gating ring. Alternatively, one may postulate that binding of heme acts merely to enhance the tension on the S6-RCK1 linker, perhaps modifying the passive mechanical properties of the gating ring/linker complex (Niu et al., 2004). This greater tautness is expected to increase open probability at negative voltages in the absence of Ca^{2+}, thereby increasing L_0 in the HCA model. However, the idea that heme simply increases the tension in the S6-RCK1 linker fails to account for the critical observation that heme modifies voltage-dependent gating, altering the steepness of the G–V (Fig. 6). The G–V steepness remains unaltered when the tension on the S6-RCK1 linker is changed by insertion/deletion mutations in the S6-RCK1 segment (Niu et al., 2004).

Physiological Implications

The Slo1 channel is influenced by heme over a broad range of divalent cation concentrations. Therefore, heme is poised to act as a regulator of the channel function under a variety of physiological conditions. Information on dynamic changes in intracellular heme concentrations is not available but it is often speculated that the concentration may increase appreciably following hemorrhaging strokes (Wagner and Dwyer, 2004). Intracellular heme then may bind to Slo1 BK channels, modulating those physiological processes dependent on BK channels, such as vasorelaxation (Patterson et al., 2002) and oxygen sensing (Williams et al., 2004). Potential inhibition of BK channels by heme may account for the cerebral vasospasm frequently observed following hemorrhaging strokes (Aihara et al., 2004). However, the possibility that heme may play a regulatory or compensatory role during these vascular accidents cannot be excluded because heme actually enhances the channel activity at more hyperpolarized, and potentially more physiological, voltages. Future studies using native BK channels should provide further insights.

We thank Dr. X. Rong for cell culture and Drs. X. D. Tang, M. Reynolds, and L.C. Santarelli for discussion.

This work was supported in part by National Institutes of Heath (F. Horrigan and T. Hoshi), American Heart Association (T. Hoshi), and Interdisziplinaeres Zentrum fuer klinische Forschung/Thueringer Ministerium fuer Wissenschaft, Forschung und Kunst B307-04004 (S.H. Heinemann).

David C. Gadsby served as editor.

Submitted: 1 February 2005
Accepted: 13 May 2005

REFERENCES

Aihara, Y., B.S. Jahromi, R. Yassari, E. Nikitina, M. Agbaje-Williams, and R.L. Macdonald. 2004. Molecular profile of vascular ion channels after experimental subarachnoid hemorrhage. *J. Cereb. Blood Flow Metab.* 24:75–83.

Aldrich, R.W., D.P. Corey, and C.F. Stevens. 1983. A reinterpretation of mammalian sodium channel gating based on single channel recording. *Nature.* 306:436–441.

Armstrong, C.M. 2003. Voltage-gated K channels. *Sci STKE.* 2003: re10.

Avdonin, V., B. Nolan, J.M. Sabatier, M. De Waard, and T. Hoshi. 2000. Mechanisms of maurotoxin action on Shaker potassium channels. *Biophys. J.* 79:776–787.

Avdonin, V., X.D. Tang, and T. Hoshi. 2003. Stimulatory action of internal protons on Slo1 BK channels. *Biophys. J.* 84:2969–2980.

Cox, D.H., J. Cui, and R.W. Aldrich. 1997. Allosteric gating of a large conductance Ca-activated K^+ channel. *J. Gen. Physiol.* 110: 257–281.

Cui, J., and R.W. Aldrich. 2000. Allosteric linkage between voltage and Ca^{2+}-dependent activation of BK-type mslo1 K^+ channels. *Biochemistry.* 39:15612–15619.

Cui, J., D.H. Cox, and R.W. Aldrich. 1997. Intrinsic voltage dependence and Ca^{2+} regulation of mslo large conductance Ca-activated K^+ channels. *J. Gen. Physiol.* 109:647–673.

Garrick, M.D., D. Scott, D. Kulju, M.A. Romano, K.G. Dolan, and L.M. Garrick. 1999. Evidence for and consequences of chronic heme deficiency in Belgrade rat reticulocytes. *Biochim. Biophys. Acta.* 1449:125–136.

Horrigan, F.T. 2005. Mg^{2+} increases the coupling of voltage-sensor activation to channel opening in BK potassium channels. *Biophys J.* 88:a.

Horrigan, F.T., and R.W. Aldrich. 1999. Allosteric voltage gating of potassium channels II. mslo channel gating charge movement in the absence of Ca^{2+}. *J. Gen. Physiol.* 114:305–336.

Horrigan, F.T., and R.W. Aldrich. 2002. Coupling between voltage sensor activation, Ca^{2+} binding and channel opening in large conductance (BK) potassium channels. *J. Gen. Physiol.* 120:267–305.

Horrigan, F.T., J. Cui, and R.W. Aldrich. 1999. Allosteric voltage gating of potassium channels I. mslo ionic currents in the absence of Ca^{2+}. *J. Gen. Physiol.* 114:277–304.

Hoshi, T. 1995. Regulation of voltage dependence of the KAT1 channel by intracellular factors. *J. Gen. Physiol.* 105:309–328.

Hu, L., J. Shi, Z. Ma, G. Krishnamoorthy, F. Sieling, G. Zhang, F.T. Horrigan, and J. Cui. 2003. Participation of the S4 voltage sensor in the Mg^{2+}-dependent activation of large conductance (BK) K^+ channels. *Proc. Natl. Acad. Sci. USA.* 100:10488–10493.

Jain, R., and M.K. Chan. 2003. Mechanisms of ligand discrimination by heme proteins. *J. Biol. Inorg. Chem.* 8:1–11.

Jiang, Y., A. Lee, J. Chen, M. Cadene, B.T. Chait, and R. MacKinnon. 2002. The open pore conformation of potassium channels. *Nature.* 417:523–526.

Magleby, K.L. 2003. Gating mechanism of BK (Slo1) channels: so near, yet so far. *J. Gen. Physiol.* 121:81–96.

Niu, X., X. Qian, and K.L. Magleby. 2004. Linker-gating ring complex as passive spring and Ca^{2+}-dependent machine for a voltage- and Ca^{2+}-activated potassium channel. *Neuron.* 42:745–756.

Padmanaban, G., V. Venkateswar, and P.N. Rangarajan. 1989. Haem as a multifunctional regulator. *Trends Biochem. Sci.* 14:492–496.

Patterson, A.J., J. Henrie-Olson, and R. Brenner. 2002. Vasoregulation at the molecular level: a role for the β1 subunit of the calcium-activated potassium (BK) channel. *Trends Cardiovasc. Med.* 12:78–82.

Ponka, P. 1999. Cell biology of heme. *Am. J. Med. Sci.* 318:241–256.

Rodgers, K.R. 1999. Heme-based sensors in biological systems. *Curr. Opin. Chem. Biol.* 3:158–167.

Rothberg, B.S. 2004. Allosteric modulation of ion channels: the case of maxi-K. *Sci STKE.* 2004:pe16.

Rothberg, B.S., and K.L. Magleby. 2000. Voltage and Ca^{2+} activation of single large-conductance Ca^{2+}-activated K^+ channels described by a two-tiered allosteric gating mechanism. *J. Gen. Physiol.* 116:75–99.

Sah, P. 1996. Ca^{2+}-activated K^+ currents in neurones: types, physiological roles and modulation. *Trends Neurosci.* 19:150–154.

Shi, J., and J. Cui. 2001. Intracellular Mg^{2+} enhances the function of BK-type Ca^{2+}-activated K^+ channels. *J. Gen. Physiol.* 118:589–606.

Swartz, K.J., and R. MacKinnon. 1997. Hanatoxin modifies the gating of a voltage-dependent K^+ channel through multiple binding sites. *Neuron.* 18:665–673.

Tang, X.D., H. Daggett, M. Hanner, M.L. Garcia, O.B. McManus, N. Brot, H. Weissbach, S.H. Heinemann, and T. Hoshi. 2001. Oxidative regulation of large conductance calcium-activated potassium channels. *J. Gen. Physiol.* 117:253–274.

Tang, X.D., R. Xu, M.F. Reynolds, M.L. Garcia, S.H. Heinemann, and T. Hoshi. 2003. Haem can bind to and inhibit mammalian calcium-dependent Slo1 BK channels. *Nature.* 425:531–535.

Tang, X.D., M.L. Garcia, S.H. Heinemann, and T. Hoshi. 2004. Reactive oxygen species impair Slo1 BK channel function by altering cysteine-mediated calcium sensing. *Nat. Struct. Mol. Biol.* 11: 171–178.

Vergara, C., R. Latorre, N.V. Marrion, and J.P. Adelman. 1998. Calcium-activated potassium channels. *Curr. Opin. Neurobiol.* 8:321–329.

Wagner, K.R., and B.E. Dwyer. 2004. Hematoma removal, heme, and heme oxygenase following hemorrhagic stroke. *Ann. NY Acad. Sci.* 1012:237–251.

Williams, S.E., P. Wootton, H.S. Mason, J. Bould, D.E. Iles, D. Riccardi, C. Peers, and P.J. Kemp. 2004. Hemoxygenase-2 is an oxygen sensor for a calcium-sensitive potassium channel. *Science.* 306:2093–2097.

Worthington, M.T., S.M. Cohn, S.K. Miller, R.Q. Luo, and C.L. Berg. 2001. Characterization of a human plasma membrane heme transporter in intestinal and hepatocyte cell lines. *Am. J. Physiol. Gastrointest. Liver Physiol.* 280:G1172–G1177.

Zeng, X.H., X.M. Xia, and C.J. Lingle. 2005. Divalent cation sensitivity of BK channel activation supports the existence of three distinct binding sites. *J. Gen. Physiol.* 125:273–286.

Zhang, G., and F.T. Horrigan. 2005. Cysteine modification alters voltage- and Ca^{2+}-dependent gating of large conductance (BK) potassium channels. *J. Gen. Physiol.* 125:213–236.

Zhang, L., and A. Hach. 1999. Molecular mechanism of heme signaling in yeast: the transcriptional activator Hap1 serves as the key mediator. *Cell. Mol. Life Sci.* 56:415–426.

Zhang, X., C.R. Solaro, and C.J. Lingle. 2001. Allosteric regulation of BK channel gating by Ca^{2+} and Mg^{2+} through a nonselective, low affinity divalent cation site. *J. Gen. Physiol.* 118:607–635.